JANUARY 2014

RubberWorld

125 years

The Technical Service Magazine For The Rubber Industry

Volume 249, No. 4

Optimizing filler dispersion
from a rubber mixer using a DMA and optical methods

Variability in abrasion resistance testing
of conveyor belt cover compounds

New modified tear test

2014 International Elastomer Conference

International Elastomer Conference – International Rubber Expo information on page 60

www.rubberworld.com

Contents

Vol. 249, No. 4 January 2014

Features

16 Optimizing the filler dispersion from a rubber mixer using a DMA and optical methods

by Henry Pawlowski, Alpha Technologies, and Dean Chamis, Blachford RP Corp. Batches from various mixer configurations were characterized, and data analyzed, to determine whether the use of a DMA and a Dispergrader can help provide an optimized mixing configuration.

25 Variability of abrasion resistance testing of conveyor belt cover compounds

by Matthew D. Goodrich, Fenner Dunlop Americas. Factors affecting the level of variation seen in abrasions testing are highlighted and discussed.

31 New modified tear test

by Edward R. Terrill and Thomas Upton, Akron Rubber Development Laboratory. A method to prepare tear test specimens from tires and molded rubber goods has been developed and appears to yield good results.

Cover photo: Courtesy of Alpha Technologies

34 Instrumentation and testing laboratories directories

Directories provide products, services and contact information for independent testing laboratories serving the rubber industry, and suppliers of rubber instrumentation and test equipment. Cross-reference grids match companies to the products and/or services they provide.

Departments

4 Editorial
5 Business Briefs
8 The Rubber Economist
10 Market Focus
12 Patent News
14 Silicone/Medical Update
61 Meetings
66 Suppliers Showcase
70 People in the News

Digital Edition Content

See the January digital edition of Rubber World for additional content not found in the print edition

- More U.S. patents
- Expanded business news
- Expanded equipment information
- Expanded instrumentation information
- Expanded materials information

Visit: www.rubberworld.com

Optimizing the filler dispersion from a rubber mixer using a DMA and optical methods

by Henry Pawlowski, Alpha Technologies, and Dean Chamis, Blachford RP Corp.

In recent years, new techniques for measuring the dispersion of fillers in rubber compounds have grown. These methods include dynamic mechanical analyzers (DMA) such as the RPA 2000 and the Dispergrader. There have been many studies to determine how to use these methods for the characterization of uncured compounds. Both methods have grown in popularity and provide much more detailed information in comparison to the traditional Mooney viscometer.

Recently, there was a need to consider the purchase of a new rubber mixer at a rubber manufacturer. The mixers of today have many options. The goal of such a purchase is to get the best possible dispersion and distribution of the ingredients from the mixer in a short period of time, and to get batches that are very uniform. This study characterized many batches from various mixer configurations. The data were analyzed to determine whether the use of a DMA and a Dispergrader can help make the correct decision for an optimized mixing configuration. Each mixer configuration was adjusted to produce the best possible mix. In this study, bad mixes were not done on purpose. So this study tried to determine those mixes that were better and those that were the best.

Equipment and experimental

Mixer

The mixer used in this study was a Kobelco 16 liter intensive mixer with accompanying TSR (twin screw roller).

The Kobelco 16 liter intensive mixer is controlled by a mixing control and monitoring system which allows the sample or trial batches to be mixed in manual (controlled by the operator) or pre-programmed automatic mode (controlled by the unit), along with it being driven by a 250 horsepower DC motor, allowing variable rotor speeds from 0-120 rpm.

The Kobelco 16 liter intensive mixer is equipped with a special gearbox that will allow either an even speed (1:1) or friction speed (1.15:1) ratio between the dual output shafts that are directly coupled to the mixer rotors. In addition, the mixer's sides, rotors and drop door can be cooled or heated using a single zone temperature control unit (water temperatures to as low as 7°C can be achieved via a chiller).

TSR

When the individual batches reach their prescribed or programmed discharge point (either time, temperature, power or a combination of any of the three), a discharge door automatically opens, releasing the batch from the mixer into a chute leading to a twin screw roller (TSR). The TSR was a 125 twin screw extruder/roller head fitted with twin 7" calender rolls.

The sides, augers and rolls of the TSR can be heated or cooled with temperature controlled water. The twin augers, which put very little extra work into the material, are driven by a 10 horsepower DC motor, achieving speeds to 30 rpm. The calender rolls are driven by a 7.5 horsepower DC motor, allowing roll speeds up to 25 rpm.

Since the TSR imparts virtually no extra work into the samples, the properties achieved are due to the work imparted by the mixer rotors, and not by any extra mixing from the TSR.

The TSR gives a sheeted product approximately 12" wide, with thicknesses ranging from 0.25" to 0.5".

Rotors

Three different types of rotors for mixing were used in this study, given their ability to impart different dispersion and distribution of ingredients during mixing. The different types of rotors used are as follows:

1. Two-wing rotors (2W).
2. Four-wing H swirl rotors (4W).
3. N rotors (N).

These different types of rotors are shown in figure 1.

Mixing

A highly filled SBR compound was used. The dominant filler was a mineral filler. All the batches that were mixed, whether done with the two-wing, the four-wing H or the N rotors, were run on the mixer in manual mode with friction speed having a 75 psi ram pressure and using 90ºF (32°C) water on the drop door, mixer sides and rotors while using the different mix cycle scenarios prescribed with only minor changes to time of addition at certain steps. Twenty batches were mixed for the two-wing trial, broken down to 10 mixes at 40 rpm, five mixes at 50 rpm and five mixes at 60 rpm. Fifteen batches were mixed for the four-wing H trial, broken down to five mixes at

Figure 1 - illustrations of the three rotor types used in this mixing study

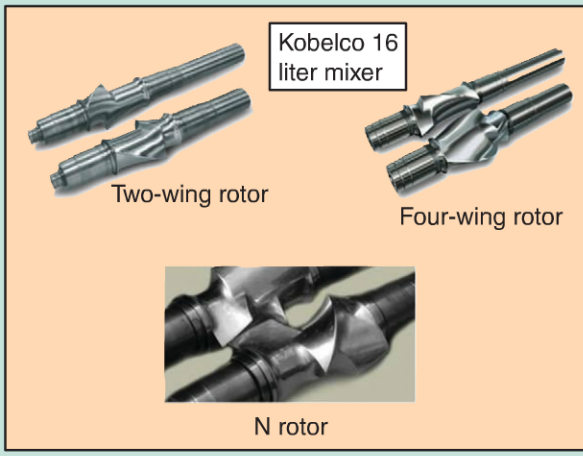

Figure 2 - biconical die configuration from the RPA 2000

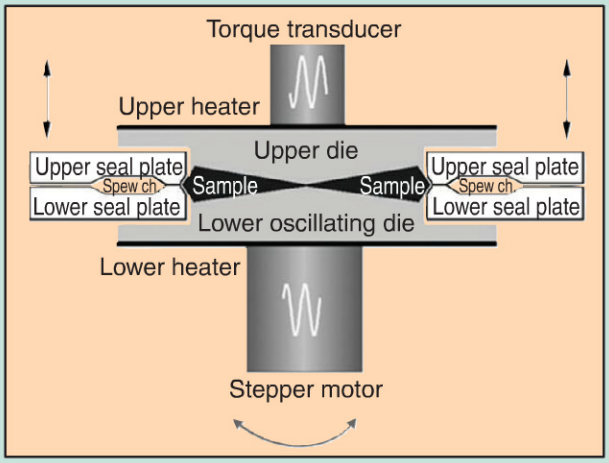

40 rpm, five mixes at 50 rpm and five mixes at 60 rpm. Similarly for the N trial, 15 batches were mixed, broken down to five mixes at 40 rpm, five mixes at 50 rpm and five mixes at 60 rpm.

Furthermore, all the batches that were mixed were converted into sheeted products via the TSR and were air cooled by hanging them directly on cooling racks. Samples for the DMA and Dispergrader testing were taken at this stage.

DMA

This testing was done with the Alpha Technologies RPA 2000 rubber process analyzer (RPA). The RPA is a dynamic mechanical analzyer, or DMA. The sample cavity of the RPA is shown in figure 2. Two biconical dies form a sample cavity of the apparatus. The die surface is grooved to hold the specimens in place and prevent slippage during testing. The outer edge of the sample cavity contains two seal plates and two seals, completely sealing the sample cavity under high pressure. A pressurized chamber helps to prevent slippage during a test. An elastomeric sample is prepared by adding sufficient volume of material either by weight or with a constant volume cutter. The sample is placed onto the lower die and then the upper die is lowered, forming the sample geometry as excess material is squeezed out. The lower die is oscillated sinusoidally at a programmable frequency and strain. The torque transducer attached to the upper die measures the force transmitted from the lower die through the sample into the upper die. The measured torque is a complex torque designated by S*.

Viscoelastic properties

A Fourier transform of the sinusoidal S* torque and strain data from the RPA separates the torque signal into elastic and viscous components. The torque signal that is in phase with the strain is the elastic component, or S'. The torque signal that is 90° out of phase with strain is the loss component or S". The die dimensions and strain are used with appropriate rheological equations to convert torque to shear modulus (G', G" and G*). The G' is a measure of the elastic or solid behavior, while the G" is a measure of the viscous or liquid behavior. The complex shear modulus G* is a measure of the combined resistance to deformation from the solid and liquid response. The tan δ is the ratio of the viscous shear modulus G" to the elastic shear modulus G' or G"/G'. The tan δ value is a useful measure to predict the processability of rubber materials. The value of tan δ will change with temperature, strain and frequency of oscillation, so comparisons must be made at the same test conditions. Usually, materials with lower tan δ values will be more difficult to process or have less scorch safety.

ASTM International Standard D6204 for mixed stocks

Table 1 shows the test conditions that are used to test the processability of mixed stocks using ASTM D6204, Parts A and B. The S* (or G*) value at 0.1 Hz and 7% strain has been shown to correlate to the Mooney viscosity of elastomers (ref. 1).

MDR 2000

One of the most popular rubber instruments used to determine the quality of a rubber mixer is the MDR 2000 curemeter. In this study, a sample of each mix is tested with the MDR 2000 for comparison. The ML (minimum S' before cure) and the MH (maximum S' during cure) are checked as measures of processability.

Dispergrader

The Dispergrader is a reflected light microscope designed to measure the dispersion of carbon black or other fillers in mixed rubber compounds. This device meets the new ASTM Standard D7723. The system uses the highlights cast by agglomerates present in a freshly cut sample surface. The amount of dispersion can be quantified with standard images or by image analysis. There are no standard images available to estimate dispersion of the materials mixed in this study. This study used image analysis to quantify dispersion by determin-

Figure 3 - Dispergrader view of a batch of uncured material mixed with the two-wing rotor at 60 rpm

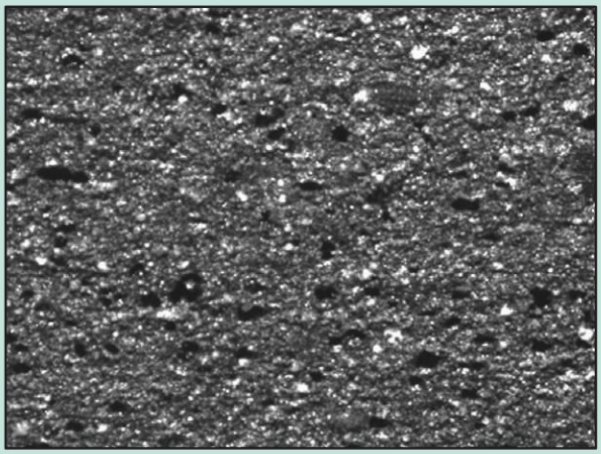

Table 1 - ASTM D6204 processability test configuration for mixed stocks

Part	*Subtest number*	*Subtest type*	*Temperature °C*	*Strain %*	*Frequency Hz*	*Time min.*
Conditioning	1	Timed	100	2.79	0.5	2
A	2	Frequency sweep	100	7.00	0.1 2 20	
B	3	Frequency sweep	100	100.00	0.1 1	

ing the number of particulates at specific sizes. Dispersion is considered improved when the number of particles at smaller sizes increases, while the number of larger particles is reduced. These particles appear white in the image. Dispersion is also improved when the total white area is reduced significantly. Mixed batches are considered uniform if the mixer produces the same dispersion level batch to batch.

Results and discussion

Dispergrader data

Table 2 contains the information about the batches mixed in this study. Figure 3 shows an image from the Dispergrader obtained from one of the batches mixed with the two-wing rotor at 60 rpm. The four-wing rotor produced a similar image. Figure 4 shows an image from a batch mixed with the N rotor at 60 rpm. Figure 4 appears to have more white particles that have a smaller size than the image in figure 3.

The Dispergrader also performed image analysis on these images. The dispergrader determined the number of agglomerates with various sizes ranging form 2.9 µm to 60 µm. The resulting histogram of the image from the two-wing rotor at 60 rpm in figure 3 is shown in figure 5, which shows the frequency of different particle sizes. The data from several histograms are combined in figure 6 for comparison. Figure 6 shows that the winged rotors produce a similar distribution of particles, while the N rotor produces more smaller agglomerates.

The dispersion is considered good when the amount of white area in the image is reduced. As shown, the white area can be in small particles or large particles. Table 2 also shows the dispersion calculated by the Dispergrader. The higher the value, the better the dispersion. Figure 7 shows a line plot of the dispersion measured by the optical method, with image analysis plotted against the various mixing configurations. The plot includes the variation calculated as 2.8 (standard deviation). The results show that the average dispersion is similar for batches from the two-wing and the four-wing configuration. There is a slight increase in dispersion with an increase in rotor speed. The N rotor produces poorer dispersion, but the mixes are more uniform.

The data in table 2 show that in order for the mixer to get to a good dispersion at lower rpm, one must increase the mixing time. The N rotor appeared to produce slightly less dispersion, but it produced very uniform batches in a shorter time.

DMA

Figure 8 shows the average G* data and variation at 0.1 Hz, 7% strain and 100°C measured by the RPA 2000. The results are shown from all mixer configurations. The N rotor at 40 rpm and 50 rpm produces higher average G* values with less variation from batch to batch. A previous study (ref. 2) showed that the longer an elastomer is mixed, the lower the resulting G* values. So this suggests that the N rotor is not mixing as much as the winged mixers. This agrees with the

Figure 4 - Dispergrader view of a batch of uncured material mixed with the N rotor at 60 rpm

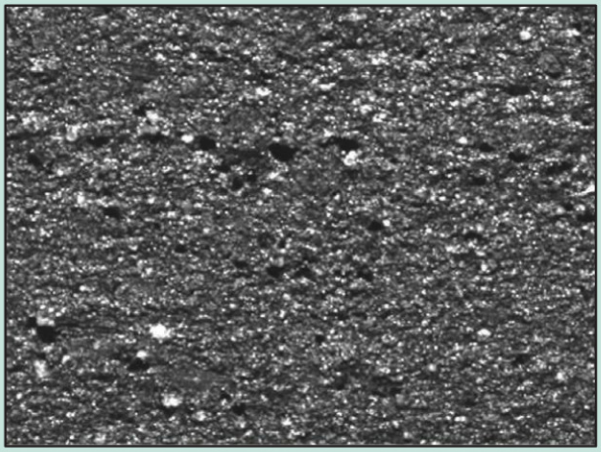

Figure 5 - image analysis of the image in figure 3 for a batch mixed with the two-wing rotor at 60 rpm - the histogram shows the count for various agglomerate sizes

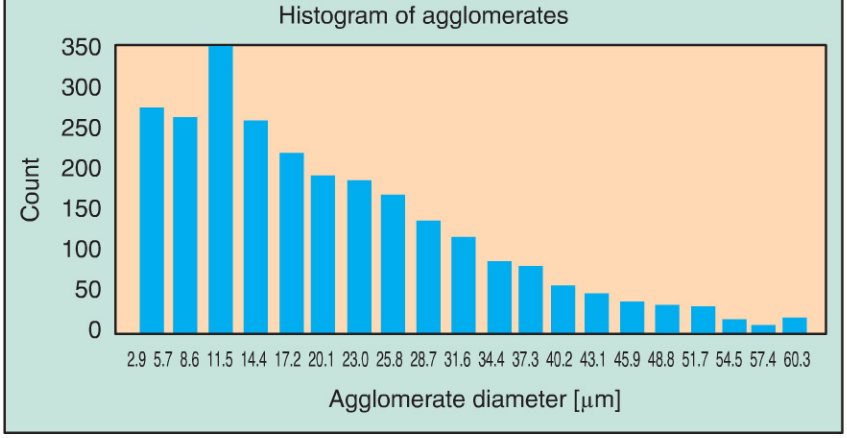

Table 2 - mixer information for the compounds in this study

Batch	Type	Rotor speed (rpm)	Ram press. (psi)	Drop temp. (°F)	Cycle time (sec)	Energy use (kwh/lb.)	ML 1+4 100°C (MU)	Alphaview dispersion (%)
1	Two-wing	40	75	240	220	0.02415	57.09	78.6
2	Two-wing	40	75	240.7	241	0.02348	62.65	77.9
3	Two-wing	40	75	239.4	261	0.02311	56.73	71.4
4	Two-wing	40	75	241.7	227	0.02444	56.29	86.5
5	Two-wing	40	75	240.8	238	0.02315	58.11	74.6
6	Two-wing	40	75	240.4	221	0.02355	58.14	75.4
7	Two-wing	40	75	241.7	235	0.02252	66.79	70.2
8	Two-wing	40	75	239.7	230	0.02337	64.14	70.7
9	Two-wing	40	75	241.6	226	0.02373	63.64	79.1
10	Two-wing	40	75	241	218			
11	Two-wing	50	75	242.6	198	0.02400	63.2	82.1
12	Two-wing	50	75	240.3	187	0.02188	65.16	75
13	Two-wing	50	75	241	194	0.02141	60.58	78
14	Two-wing	50	75	242.3	188	0.02211	59.26	74
15	Two-wing	50	75	240.5	199	0.02261	58.57	81.1
16	Two-wing	60	75	241.9	167	0.02154	60.69	74
17	Two-wing	60	75	241.4	170	0.02165	59.67	80
18	Two-wing	60	75	241.2	167	0.02116	58.56	74.1
19	Two-wing	60	75	242.5	170	0.02224	57.54	78.2
20	Two-wing	60	75	241.8	168	0.02147	59.95	91
21	Four-wing	40	75	240.4	169	0.02199	65.37	68.3
22	Four-wing	40	75	238.9	175	0.02201	58.46	69.9
23	Four-wing	40	75	240	174	0.02231	64.87	79.9
24	Four-wing	40	75	239.7	182	0.02215	58.61	72.1
25	Four-wing	40	75	240.4	177	0.02242	63.1	73.2
26	Four-wing	50	75	241	148	0.02106	59.7	71.6
27	Four-wing	50	75	241.7	149	0.02124	66	78.3
28	Four-wing	50	75	241.4	149	0.02125	61.01	71
29	Four-wing	50	75	240.9	148	0.02121	62.05	83.1
30	Four-wing	50	75	241.8	152	0.02127	65.05	78.6
31	Four-wing	60	75	241.9	134	0.02136	65.77	76.1
32	Four-wing	60	75	241.4	134	0.02078	59.86	
33	Four-wing	60	75	240.9	134	0.02064	59.51	79.2
34	Four-wing	60	75	242.1	133	0.02104	59.98	78.1
35	Four-wing	60	75	241.2	134	0.02118	59.42	82.1
36	N rotor	40	75	240	177	0.02221	61.73	67.1
37	N rotor	40	75	241	172	0.02159	64.78	68.9
38	N rotor	40	75	241	171	0.02189	65.37	69.1
39	N rotor	40	75	239	170	0.02136	64.04	69.3
40	N rotor	40	75	240	174	0.02174	66.8	68.9
41	N rotor	50	75	241	147	0.02111	64.62	68.6
42	N rotor	50	75	241	147	0.02169	65.71	68.2
43	N rotor	50	75	242	152	0.02186	66.2	69.8
44	N rotor	50	75	242	151	0.02122	65.05	70.5
45	N rotor	50	75	242	151	0.02150	64.14	68
46	N rotor	60	75	241	137	0.02066	59.62	69.9
47	N rotor	60	75	242	137	0.02098	64.17	68.2
48	N rotor	60	75	242	135	0.02094	65.12	70.2
49	N rotor	60	75	240	136	0.02077	59.54	70.7
50	N rotor	60	75	241	135	0.02092	64.62	69.3

dispersion measured by the Dispergrader, but the image from the Dispergrader on N rotor batches does show an increase in the number of smaller agglomerates.

Figure 9 shows a line plot with tan δ from each mixer configuration. The results show that the highest average tan δ is produced by the four-wing rotor at 60 rpm. The N rotor produces the lowest average tan δ at 40 and 50 rpm, indicating the least amount of work was put into the mix, which is in agreement with its value of G*. The same study (ref. 2) showed that, as mixing time increases, the tan δ value increases. The variation of batches with the N rotor appeared to increase significantly as the rpm increased.

Figure 10 shows the results for G* from D6204 Part B or 100% strain at 0.1 Hz and 100°C. The results show that G* at the higher strain/higher frequency follows a similar pattern as the results at 0.1 Hz and 7%, shown in figure 8.

Figure 11 shows the results for tan δ from Part B at 100% strain and 0.1 Hz. These results appeared to follow the ranking of tan δ at 7% strain in figure 9. The results from Part B did not appear to show any significantly different information on these batches compared with the results from Part A.

Figure 12 shows the correlation of Mooney viscosity of a batch versus the G* at 100°C, 7% strain and 0.1 Hz. Results show a good correlation with some scatter in the data. Note that some of the mixer configurations produce a tight spread of data, while others cover the full range of variation seen in the mix study. The N rotor at lower rpm appears to have the least variation in data, as also seen in the line plots.

One DMA measure that is supposed to indicate dispersion is to calculate the ratio of the G' modulus at low strain to the G' at high strain (ref. 3). The ratio of (G' high strain)/(G' low strain) should indicate dispersion with higher values indicating better dispersion. Note that, typically, the low strain is done at 1% strain and the higher strain is 10% strain. These conditions are not available in the D6204AB test. The G' value at 7% is used for the low strain, and G' at 100% is used for the high strain in this study. Figure 13 shows the results from the mixes in this study. The results indicate that the best average dispersion occurs with the N rotor at 60 rpm. However, these results appear to also have much variation. The four-wing rotor at 40 rpm had slightly less variation, but more uniform batches than the N rotor.

Figure 6 - histograms from various batches produced with different rotors and speeds plotted together for comparison - the two-wing and four-wing histograms are similar - the N rotor histograms show more smaller agglomerates

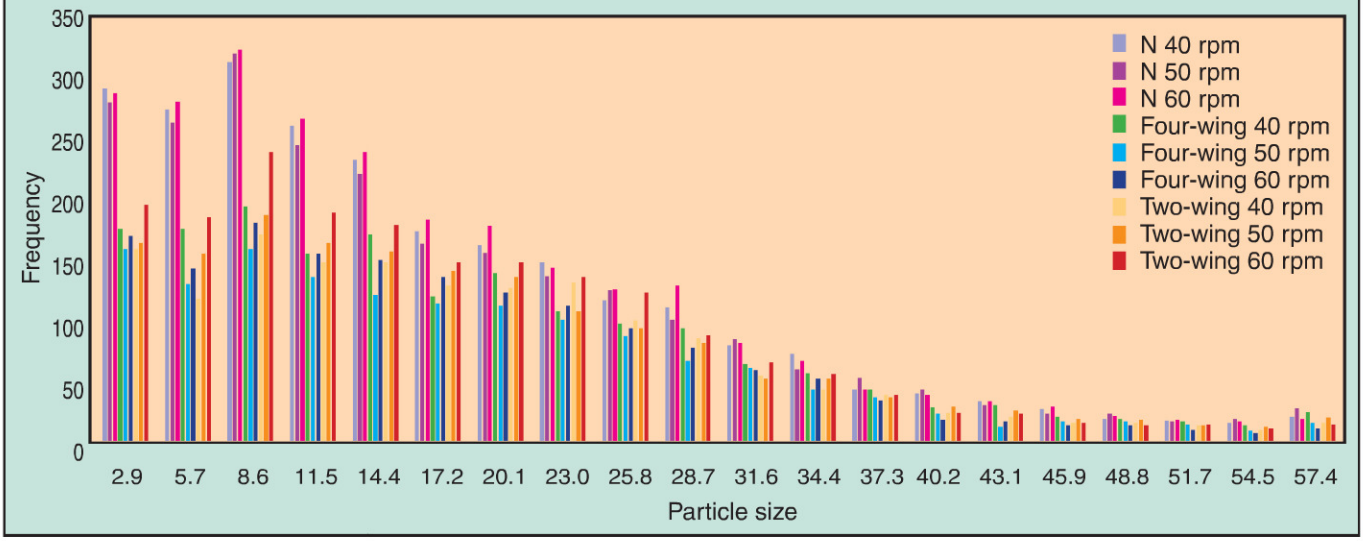

Figure 14 shows a line plot of mixing time versus mixing configuration. The results show that there is a large range of times, depending on the mixer configuration. This plot also shows that many times the better dispersion occurs in the mixer configuration that has the longer mixing time.

Figure 15 shows the amount of power put into the material. This appears to follow the mixing time plot of figure 14.

Figure 16 shows the ML measured by an MDR 2000. The results show that it is difficult to separate the results from the winged rotors. The N rotor produces a higher ML, probably due to the shorter mixing time. Figure 17 shows similar results for MH. These results show that the average MH value covers a very narrow range, except for the results from the two-wing rotor at 40 and 50 rpm. Those results show that the batch to batch variation with the two-wing rotor is quite large compared with the other mixer configurations. This plot also shows that the MH value is not very sensitive to mixer configuration.

There are alternate ways to view the RPA dynamic data

Figure 7 - average % dispersion and variation in % dispersion from multiple batches of all mixer configurations

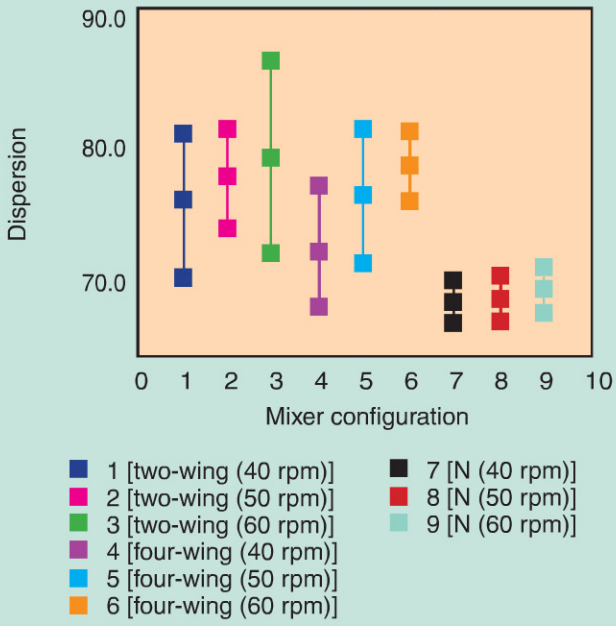

Figure 8 - G* at 0.1 Hz, 100°C and 7% strain measured on the uncured mixes

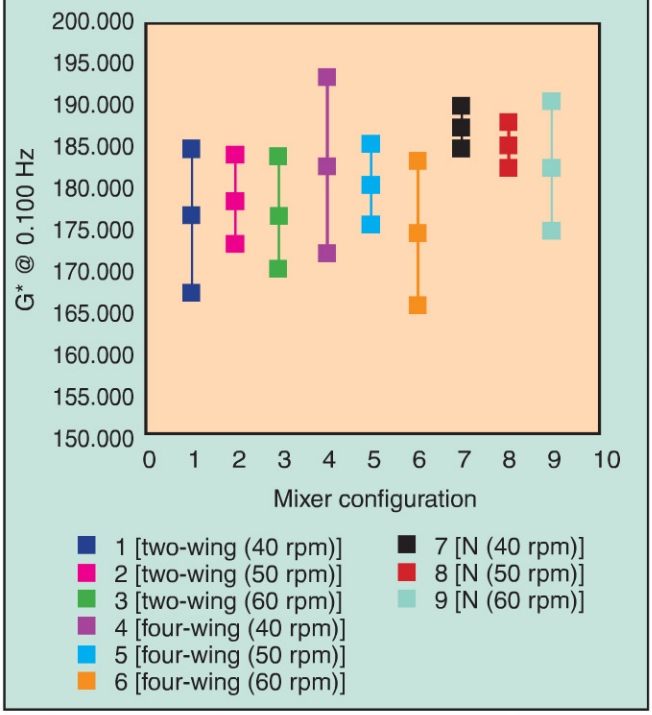

Figure 9 - tan δ at 100°C, 0.1 Hz and 7% strain - higher values typically indicate longer mix times

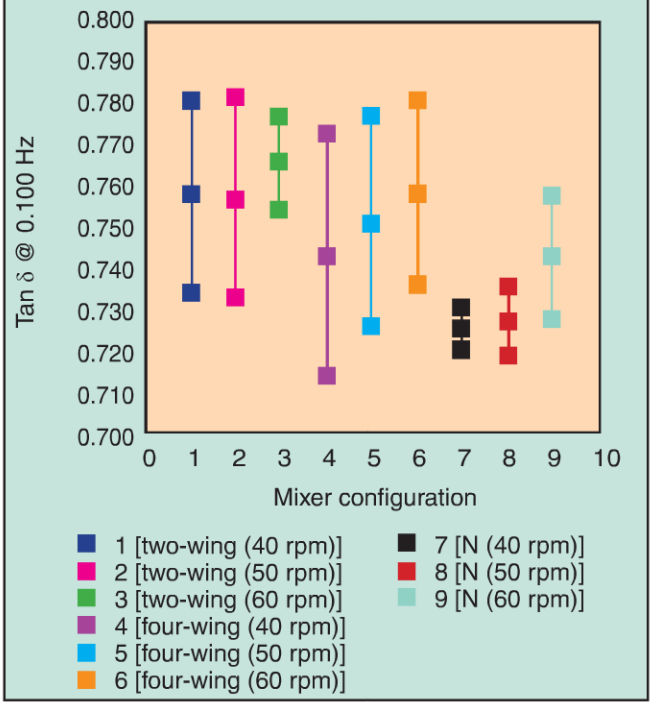

Figure 11 - tan δ at 0.1 Hz, 100°C and 100% strain

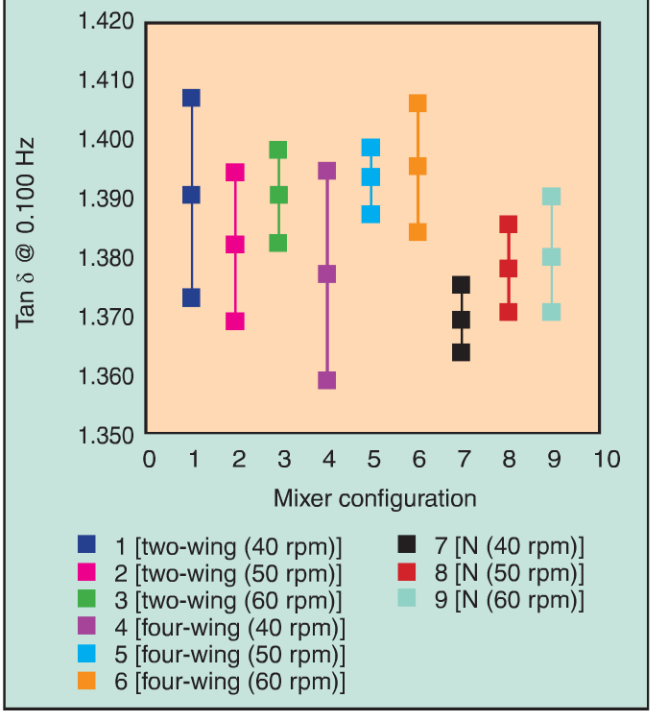

from this study. The G* or viscosity value can be plotted on the x-axis against the tan δ value on the y-axis. The results are shown in figure 18. Typically, as mixing time increases, the expectation is that G* will decrease and tan δ will increase so the mix result will move from the lower right to the upper left. This is the direction of the majority of the stocks plotted in

Figure 10 - G* at 0.1 Hz, 100°C and 100% strain

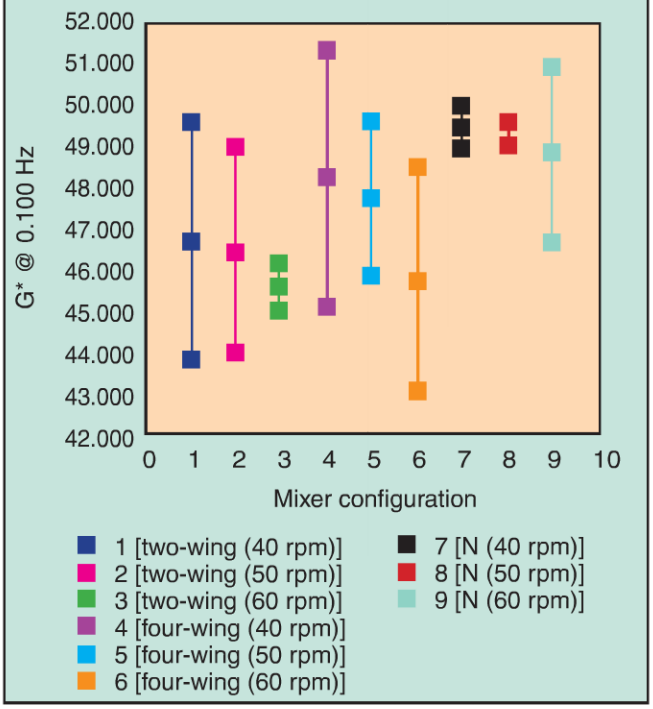

Figure 12 - correlation of Mooney viscosity and G* at 0.1 Hz, 7% strain and 100°C - results show the expected trend with some scatter

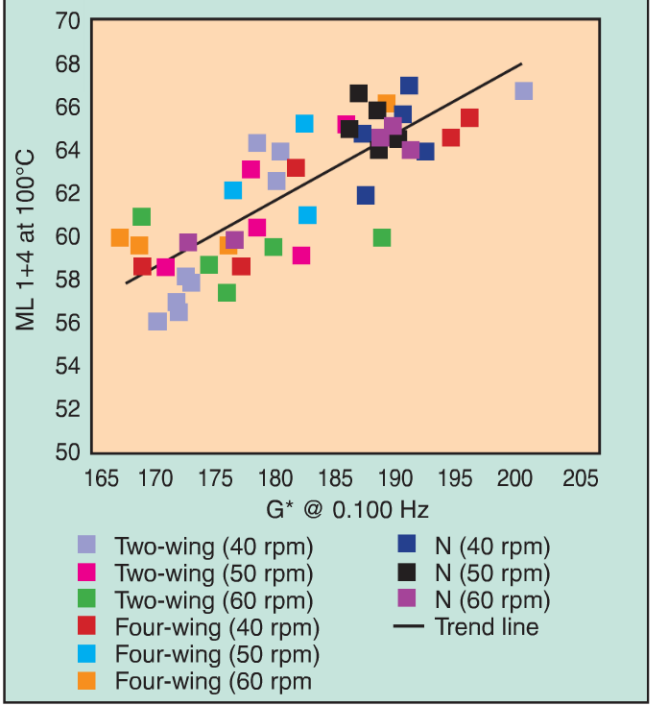

Figure 13 - the ratio of G' at high strain to the G' at low strain - higher values should indicate better dispersion

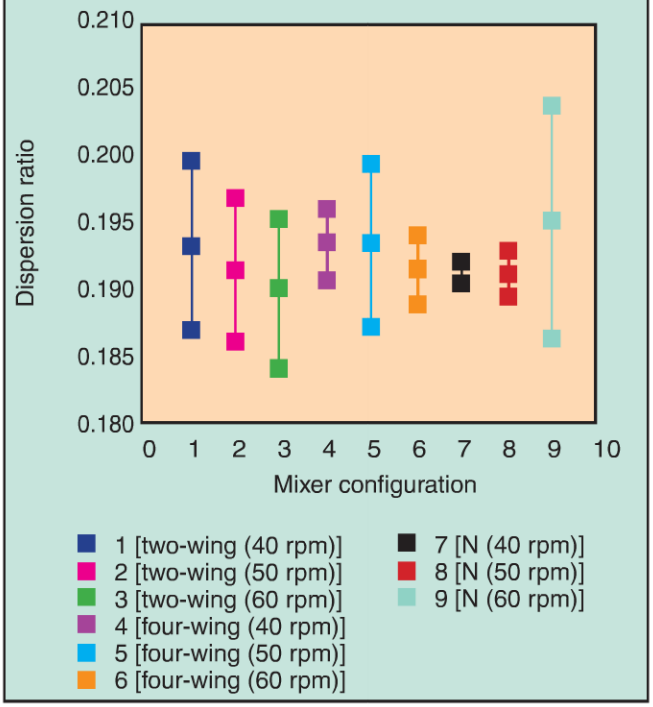

figure 18. The N rotor mixes tend towards the lower right, while the two-wing rotor tend towards the upper left. This is in good agreement with the amount of mixing time. Several of the mix configurations show a good batch uniformity. These

Figure 14 - mixing time from each mixer configuration

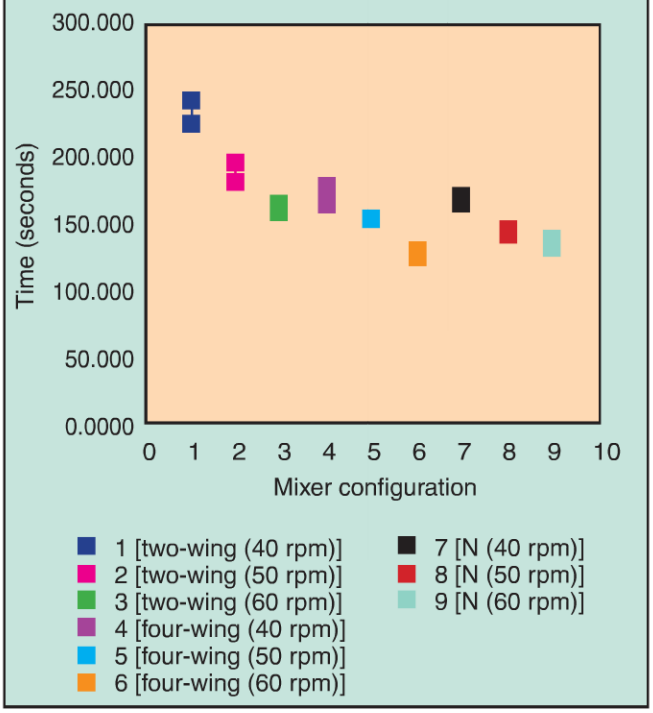

Figure 15 - power input into a mix versus the mixer configuration - the two-wing mixer required more power to get a good mix

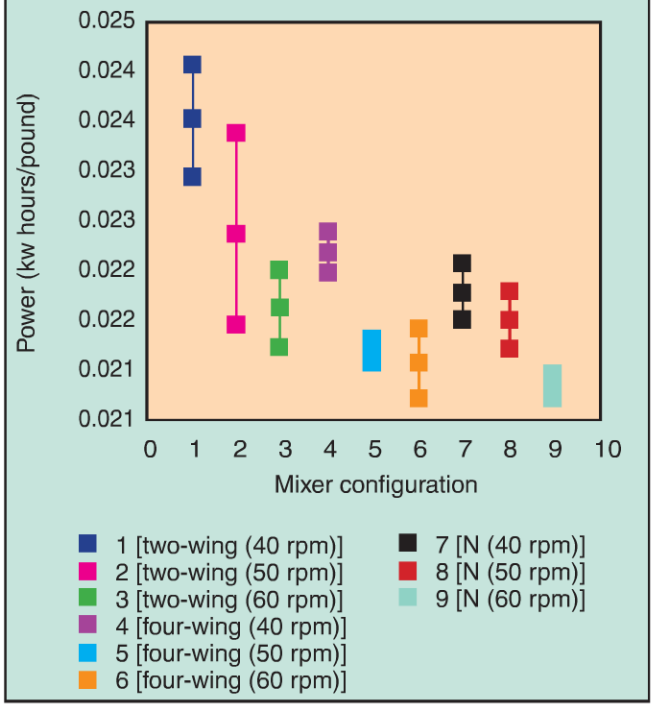

especially include the N rotor mixes.

Another alternate plot is to put G' on the x-axis and G" on the y-axis, as shown in figure 19. This is a modification of a

Figure 16 - ML value from an MDR - results from the winged mixers are very close - the N rotor ML is significantly higher

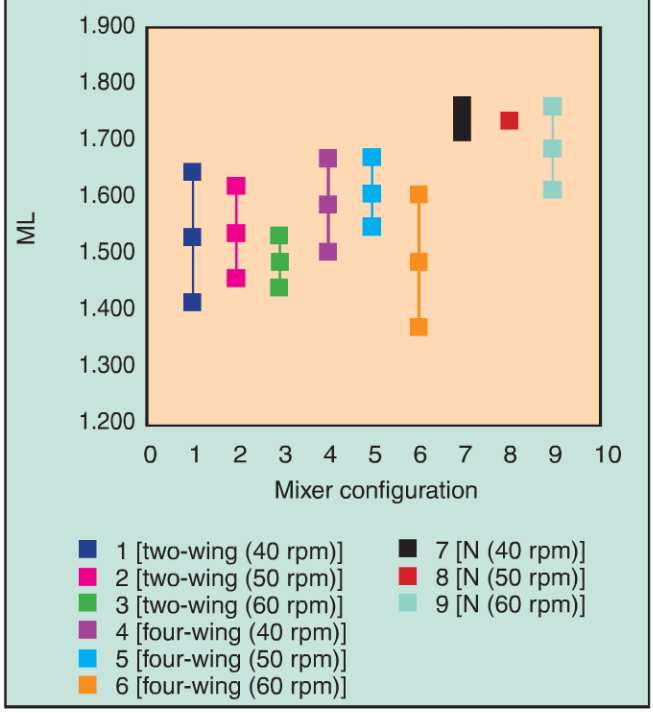

Figure 17 - MH values from all mixes using an MDR - results show a very narrow range of values except for the two-wing mixer at 40 and 50 rpm

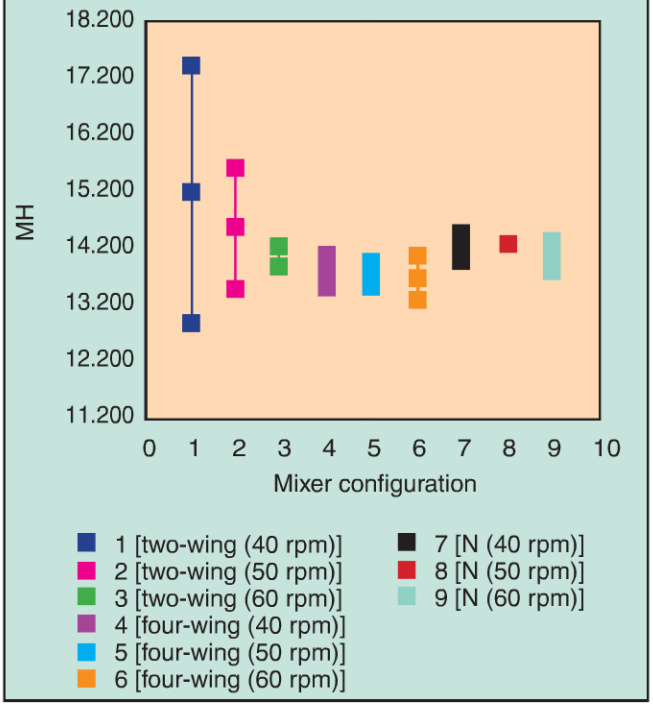

Figure 18 - plot of G* at 20 Hz, 100°C and 7% strain versus the corresponding tan δ

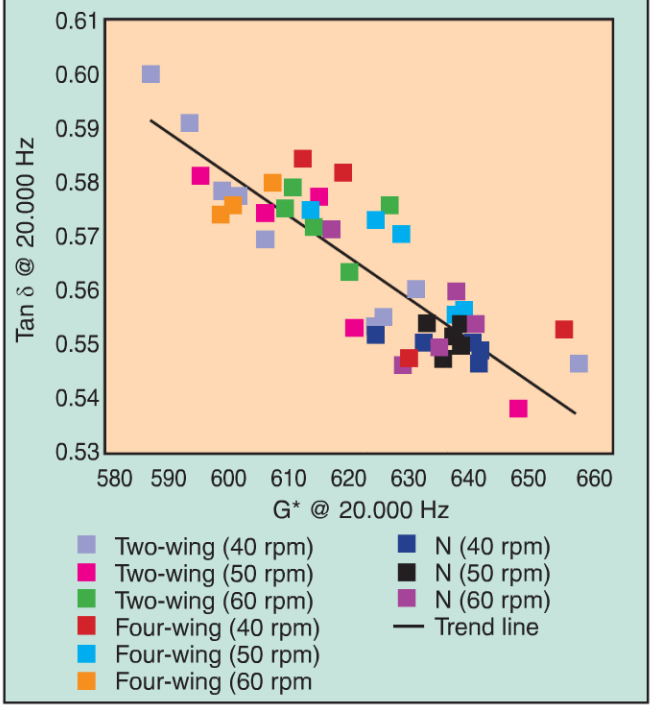

Cole-Cole plot. This result shows a linear relationship with some scatter. As the amount of mixing increases, the values of G' and G" decrease. The corresponding location of each mix

Figure 19 - G' at 0.1 Hz, 100°C and 7% strain versus the corresponding G" value

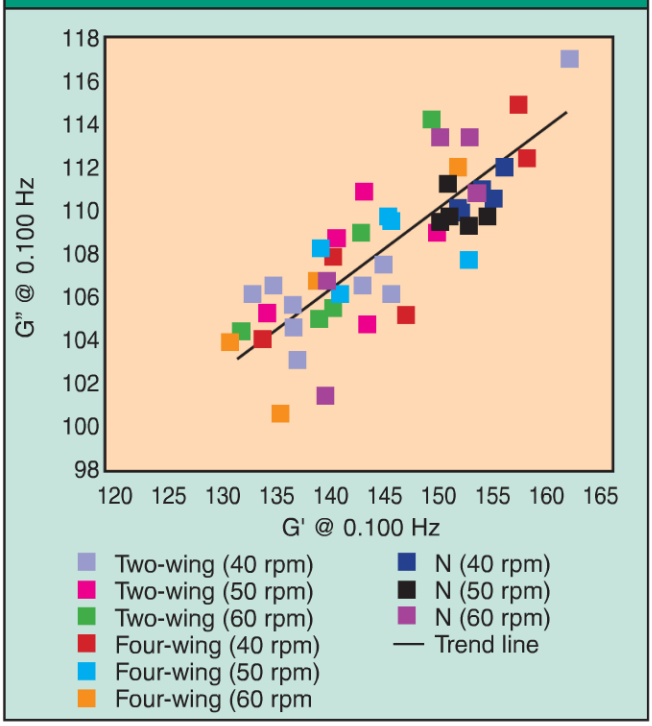

Figure 20 - a plot of G' versus G" at 0.1 Hz, 100°C and 100% strain - all of the results are close to a single line

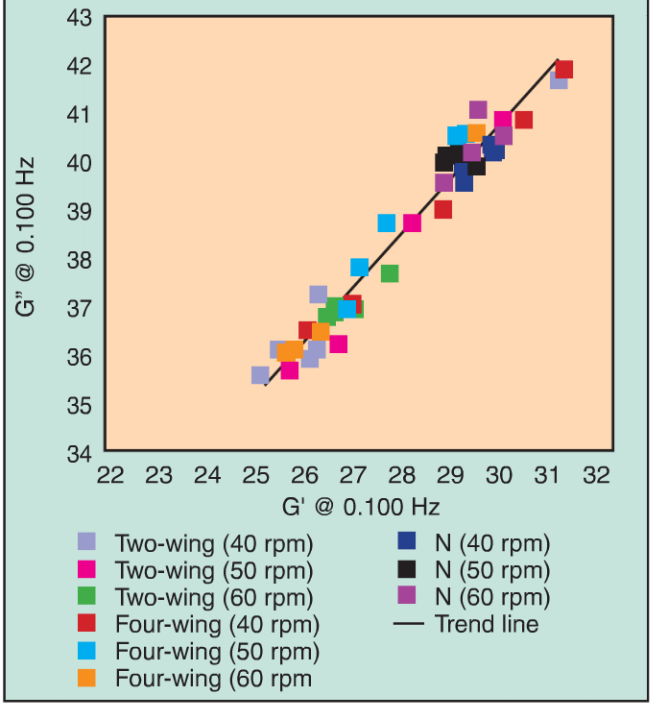

is also predicted by the amount of mix time. This plot is a good way to rank the actual amount of work put into the material, even though the mixer configurations are quite different.

(continued on page 33)

Figure 11 - side view of tear path in molded groove specimen

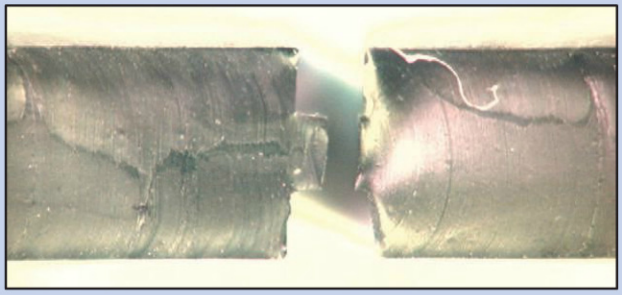

Figure 12 - side view of tear path in machined groove specimen

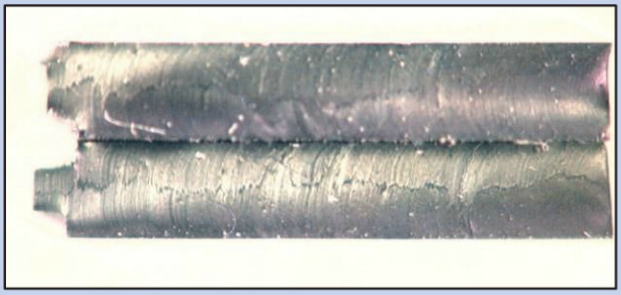

grooved tear specimens were obtained from slices extracted from tires. The specimen thickness was 2 mm (80 mils) with 0.5 mm (20 mils) groove on each side. The test results were compared to the results from molded groove tear test specimens. The results were very similar to molded groove trouser tear (figure 6), although the machine groove had larger variation than the molded groove. Figures 7 and 8 show that similar raw data curves (force versus deflection) were obtained. Figures 9 and 10 show that both specimens have smooth grooves located centered one above the other, which is specified in ASTM D624. Figures 11 and 12 show that both specimens had tears which propagated vertically between the grooves. These results were obtained for an SBR based compound. Based on prior work, this compound was expected to yield a torn surface inclined at an angle to the vertical (ref. 1).

Conclusion

A method to prepare tear test specimens from tires and molded rubber goods has been developed and appears to yield good results.

This article is based on a paper presented at the 184th Technical Meeting of the Rubber Division, ACS, October 2013.

Reference

1. A. Ahagon, A.N. Gent, H.J. Kim and Y. Kumagai, "Fracture energy of elastomers in Mode I (cleavage) and Mode III (lateral shear)," Rubber Chemistry and Technology, 48, 896-901 (1975).

Optimizing filler dispersion

(continued from page 23)

Figure 20 shows a similar plot as figure 19 using the G' and G" value at 100% strain and 0.1 Hz. The results are very linear with much less scatter. This test condition appears to be the best indicator of the relative amount of work put into the mix.

Conclusions

A series of good rubber batches was mixed using nine different mixer configurations. The dispersion and uniformity of these batches were measured using optical methods and DMA methods. The optical methods showed that the better dispersion is produced by mix configurations that increase the amount of time in the mixer. This is confirmed by the DMA methods. The rubber manufacturer in this study is able to use this information in order to decide whether they prefer: (1) better dispersion and shorter mix cycle time with the four-wing H swirl rotors [4W], (2) best dispersion and longer mix cycle time with the two-wing rotors [2W], or (3) best uniformity and shorter mix cycle time with the N rotor [N].

This article is based on a paper presented at the 184th Technical Meeting of the Rubber Division, ACS, October 2013.

References

1. H. Pawlowski and J. Dick, "Viscoelastic characterization of rubber with a new dynamic mechanical tester," presented at a meeting of the Akron Rubber Group in Akron, OH, April 23, 1992.

2. J. Dick and H. Pawlowski, "Applications for the rubber process analyzer," paper no. 37, presented at a meeting of the Rubber Division, ACS, in Nashville, TN, November 3-6, 1992.

3. J. LeBlanc, "Filled polymers: Science and industrial applications," CRC Press, Boca Raton, FL, 2010.

Abrasion resistance testing

(continued from page 29)

involved in this type of testing take the time to understand the sources of variation highlighted above and the impact that those factors have on consistency of results. A thorough understanding of these cause and effect relationships will allow the operator to introduce better practices into their testing and ultimately increased consistency. With increased consistency will come higher quality data that can be shared and compared more reliably, making troubleshooting and decision making with regard to rubber quality or manufacturing issues an easier task for those involved.

This article is based on a paper presented at the 184th Technical Meeting of the Rubber Division, ACS, October 2013.

References (standards and methods)

1. DIN ISO 4649:2006-11: "Determination of Abrasion Resistance Using a Rotating Cylindrical Drum Device."

2. Zwick Materials Testing Technical Documentation Instruction Manual Dok.-Nr.F12-002 Ref. V12-006.